https://doi.org/10.29081/ChIBA.2025.629

Scientific Study & Research

Chemistry & Chemical Engineering, Biotechnology, Food Industry

ISSN 1582-540X

## ORIGINAL RESEARCH PAPER

# DYNAMIC STUDY BEHAVIOR OF THE FLUIDIZED BINARY MIXTURE BED WITH BENTONITE PARTICLES

Gabriela Muntianu<sup>1</sup>, Ileana-Denisa Nistor<sup>1\*</sup>, Ana-Maria Georgescu<sup>1</sup>, Ana-Maria Roșu<sup>1</sup>, Diana-Carmen Mirilă<sup>2, 3</sup>, Alina Monica Mareș<sup>4</sup>, Cosmin Valeriu Jinescu<sup>5\*</sup>

\*Corresponding authors: dnistor@ub.ro, cosmin.jinescu@yahoo.com

Received: December, 16, 2024 Accepted: March, 14, 2025

Abstract: This study presents experimental data on the behavior of gas-solid

systems in classical fluidization of simple particles and binary mixtures. Sodium and calcium bentonite particles with different physical properties were used to determine dynamic parameters. The use of bentonite particles is often recommended because they are easy to manipulate and have high specific surface areas for gas-solid contact. The study examines the influence of average particle diameter  $(\overline{d}_p)$  and bed height  $(H_0)$  on bed porosity  $(\varepsilon_0)$ , pressure drop  $(\Delta P)$ , and minimum fluidization velocity  $(U_{mf})$ . Bentonite particles in a fluidized bed belong to Groups B and D according to Geldart's classification. The binary mixture particles have the same diameter but different densities and are pseudo-homogeneously mixed. The minimum fluidization velocity for well-mixed particles ( $U_{mf,mix}$ ) was determined for two mixtures with 0.57 mass fraction of sodium bentonite and bed ratios  $(H_0/D)$  close to 2. Experimental values for minimum pressure drop ( $\Delta P_{min}$ ), minimum fluidization velocity ( $U_{mf}$ ), and minimum fluidization velocity for the mixture were compared with theoretical values using empirical equations. Regression analysis of all experimental data provided an empirical model for  $U_{mf}$  and  $U_{mf,mix}$ . The study aims to achieve better dynamic conditions for efficient and effective use of binary mixtures in future adsorption processes.

**Keywords:** bentonite, binary mixture, mass fraction, minimum fluidization velocity, pressure drop

## INTRODUCTION

Fluidization is an operating technique in which a solid bed (powder or granular particles), supported by a perforated plate for gas or fluid phase distribution, allows the fluidizing agent (gas or liquid) to pass through it, creating an expanded state of the gas-solid system [1]. In general, solid particles become fluidized in the bed when an ascending gas flow exerts a drag force strong enough to overcome the force of gravity. The drag force is the frictional force between the particles and the gas. The bed particles exert an equal and opposite drag force on the gas flow [2]. The surface of a bubbling fluidized bed resembles that of a boiling liquid and can be easily mixed, just like a liquid [3]. Fluidization offers multiple advantages in comparison with the fixed beds, including good gas-solid contact, particles transport, particles rapid mixing, excellent heat and mass transfer characteristics [4]. Fluidization process is present in all operations based on gas-solid contact and applications being met in chemicals, pharmaceuticals, environmental, foods [5], energy, nuclear, petrochemical, oil, coal, wood and construction materials [6].

Increasing the gas flow (Gv) through a granular bed changes the mode of gas-solid contact in many ways [7]. The five distinct stages or regimes of fluidization observable experimentally are: fixed or packed bed, incipient fluidization, bubbling fluidization, slugging, and turbulent fluidization [8]. However, not all of these regimes can be observed in all gas-solid systems, as some regimes depend on the size of the equipment used or additional components for transporting particles in pneumatic regimes or entrained particle beds.

Fluidization regimes can be classified into two categories: particulate or homogeneous fluidization [9] and bubbling or aggregative fluidization [10]. Most gas or liquid fluidized beds under normal operation exhibit particulate fluidization. In particulate fluidization, the solid particles usually disperse uniformly in the fluidizing bed without gas bubbling, resulting in quiet fluidization. The particle bed can transition from a fixed bed to a bubbling fluidized bed when the gas velocity  $(U_g)$  increases beyond the minimum fluidization velocity  $(U_{mf})$  of the gas-solid system [11]. Particulate fluidization exists between the minimum fluidization velocity  $(U_{mf})$  and the minimum bubbling velocity  $(U_b)$ . The gas velocity  $(U_g)$ , at which gas bubbles first appear in the bed particles, is known as the minimum bubbling velocity  $(U_{mb})$  [12].

The aggregative or bubbling regime is one of the most studied flow regimes in gas-solid systems. Gas bubbles join together and break up as gas flow  $(G_v)$  increases. Eventually, the gas bubbles become large enough to occupy a substantial fraction of the cross-section of the fluidization column. Under certain conditions, these elongated gas bubbles are called slugs.

The flow pattern depends exclusively on system properties such as average particle diameter  $(\overline{d}_p)$ , average particle density  $(\overline{\rho}_p)$ , particle shape or sphericity  $(\varPsi)$ , gas phase density  $(\rho_g)$ , and gas viscosity  $(\eta_g)$ . There are several criteria available to determine whether a gas-solid system will exhibit particulate fluidization (Fr < 1) or aggregative fluidization (Fr > 1) [2]. The criterion for particulate or aggregative fluidization is the value of the Froude number, presented in equation 1:

$$Fr = \frac{U_{mf}^2}{g \cdot \overline{d}_p} \tag{1}$$

where  $U_{mf}$  is the minimum fluidization velocity (m·s<sup>-1</sup>), g is the acceleration due to gravity (m·s<sup>-2</sup>), and  $\overline{d}_p$  is the average particle diameter (m). The main parameters that describe the dynamic behavior of particulate fluidization are: pressure drop ( $\Delta P$ ), gas velocity ( $U_g$ ), minimum fluidization velocity ( $U_{mf}$ ), and bed porosity ( $\varepsilon_\theta$ ).

The minimum pressure drop ( $\Delta P_{min}$ ) in the fixed bed of devices with a cross-section fluidization column is a constant and represents the gas energy consumption needed to maintain the fluidization regime. Predicting  $U_{mf}$  is essential for the transition from a fixed bed to a fluidized bed [13]. For a homogeneously porous bed, measuring the bed height ( $H_0$ ) and calculating the bed porosity ( $\varepsilon_0$ ) [14] is expressed using the empirical equation (2) obtained by Carman-Kozeny:

$$\Delta P_{\min} = g \cdot (\overline{\rho}_p - \rho_g) \cdot (1 - \varepsilon_0) \cdot H_0$$
 (2)

The minimum fluidization velocity ( $U_{mf}$ ) can be estimated in a mono-component system by first calculating the Archimedes number (Ar) [15] and then the Reynolds number in a fluidized state ( $Re_{mf}$ ) [16, 17] presented in equation 3:

$$Re_{mf} = \sqrt{33.7^2 + 0.0408 \cdot Ar} - 33.7 \tag{3}$$

Minimum fluidization velocity ( $U_{mf}$ ) can be calculated theoretically for various particle shapes [18] using the following equation:

$$U_{mf} = \frac{\eta_g \cdot \text{Re}_{mf}}{\rho_g \cdot \overline{d}_p} \tag{4}$$

where  $\eta_g$  is gas viscosity (Pa·s),  $\rho_g$  is gas density (kg·m<sup>-3</sup>), and  $\overline{d}_p$  is average particle diameter (m). For air,  $\eta_g = 18.4 \cdot 10^{-6}$  Pa·s and  $\rho_g = 1.293$  kg·m<sup>-3</sup> at 21.1°C and 1 atm. In practice, the minimum fluidization velocity ( $U_{mf}$ ) is determined using fluidization diagrams that depend on the pressure drop ( $\Delta P$ ) in the bed and the gas velocity ( $U_g$ ), represented as ( $\Delta P - U_g$ ). Geldart studied gas-solid fluidization for different types of solid particles with varying sizes and densities, from the finest to the heaviest, noting their fluidization behavior. The particles can be classified in 4 groups [19, 20]: group A includes aerated powders (e.g., catalyst granules) [21, 22], group B includes sand particles [23], group C consists of fine cohesive particles (e.g., cosmetic and talcum powder, flour, starch), and group D includes large and/or very dense particles (e.g., cereals, coffee beans, coal, clays) [24, 25].

Fluidization is an important technique for intensifying operations and industrial processes, regardless of the powder group (A to D). It offers opportunities to design, operate, and scale-up fluidized beds in new ways [4], such as using binary mixtures of particles with different diameters and/or densities.

A binary mixture of particles with different diameters and/or densities tends to separate vertically under fluidized conditions. Regardless of the particle configuration in the bed, the non-uniform distribution of the different solid components is caused by the competitive action of mixing and segregation phenomena [26].

Rowe and Nienow extensively studied binary mixture systems and classified the particles into two categories: the component that tends to settle to the bottom, called "*Jetsam*," and the component that tends to float on the fluidized bed surface, called "*Flotsam*" [27]. Chiba proposed another classification for two-solid beds with particles of different

densities [28, 29]. Generally, the high-density component will segregate to become the "Jetsam" particles, and the low-density component will be the "Flotsam" particles. However, there are exceptions. If there is no difference in density but only in diameter, large particles will be "Jetsam," and small particles will be "Flotsam." In both cases, segregation occurs [30 – 32].

Figure 1 shows the evolution of a fixed bed depending on the gas velocity for the arrangement of "Jetsam" and "Flotsam" particles in a pseudo-homogeneous configuration.

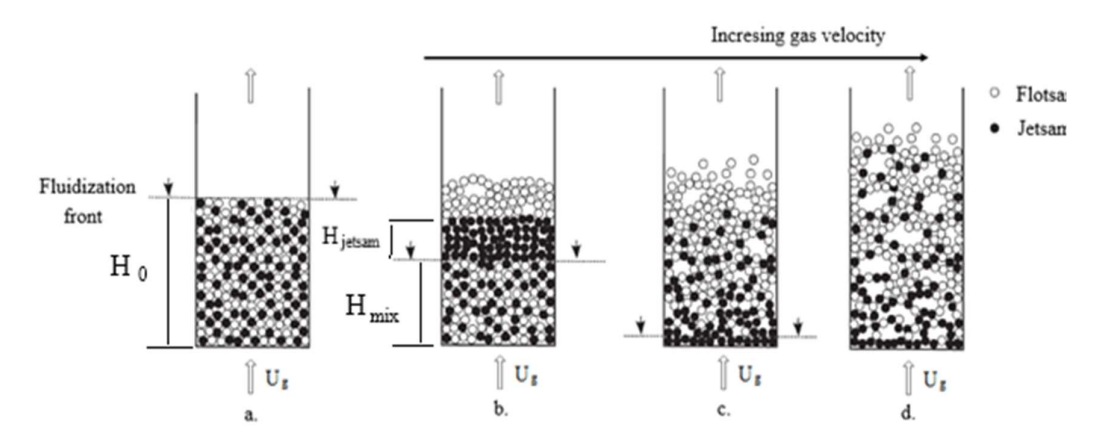


**Figure 1.** Fluidization regimes for a two-solid bed in a pseudo-homogeneous configuration: a. fixed bed; b. partially segregated bed; c. well-mixed bed; d. fully segregated bed [33].

In the case of a two-solid pseudo-homogeneous configuration, the bed structure made up of the "Flotsam" and "Jetsam" particles will change as it passes through the four fluidization regimes observable experimentally: fixed bed, partially segregated bed, well-mixed bed, and fully segregated bed [33].

During fluidization by air (at ambient conditions) for a pseudo-homogeneous configuration, as the gas flow rate increases, the fluidization front moves towards the bottom of the column until the whole bed is brought into a fluidized state [34 - 36]. At the column surface, a bubbling bed contains almost exclusively the "Flotsam" component, while the "Jetsam" particles sink and form a de-fluidized bed just behind the fluidization front [37].

In practice, the initial and total fluidization velocities ( $U_{if}$  and  $U_{tf}$ ) can be determined from the  $\Delta P_{mix}$  -  $U_g$  diagram for a mixing or segregating mixture [30, 38 – 41], along with visual observations of the bed behavior.

To estimate the minimum fluidization velocity for a binary system  $(U_{mf,mix})$ , it is necessary to consider the characteristics of the mixing particles. The main physical properties of the bi-component bed are: average particle diameter  $(\overline{d}_{p,mix})$ , average particle density  $(\overline{\rho}_{p,mix})$ , mass fraction  $(x_J)$ , volumetric fraction  $(x_{v,J})$ , and volumetric average mixture diameter  $(\overline{d}_{v,mix})$ . The average particle diameter and particle density of the mixture are calculated using the equation of weighted mass [42].

The volumetric fraction of "Jetsam" particles  $(x_{v,J})$  can be calculated using the equation 5 [43]:

$$x_{v,J} = \frac{V_J}{V_J + V_F} = \frac{V_J}{V_{total \, mixture}} \tag{5}$$

The volumetric average mixture diameter of solid particles ( $\overline{d}_{v,mix}$ ) was calculated using equation (6) by weighting the particle diameters, considering the volumetric fraction and particle shapes [24]:

$$\overline{d}_{v,mix} = d_{p,J} \cdot x_{v,J} \cdot \psi_J + d_{p,F} \cdot x_{v,F} \cdot \psi_F \tag{6}$$

It is important for the practical design of the equipment to determine the minimum fluidization velocity  $(U_{mf})$  at which single particles of "Jetsam" or "Flotsam" are completely fluidized.

The minimum fluidization velocity of the particle mixtures ( $U_{mf,mix}$ ) can be calculated using the equation of Chiba [43] for a completely segregated bed of particles with different diameters and/or densities:

$$U_{mf,mix} = \frac{U_{mf,F}}{\left(1 - x_{J}\right) \cdot \left(1 - \frac{U_{mf,F}}{U_{mf,J}}\right) + \frac{U_{mf,F}}{U_{mf,J}}} \tag{7}$$

The nouvelty of this research is the use of the bentonite particules in binary fluidized bed and the determination of the experimental and calculated dynamic parameters by equations during fluidization.

The paper presents the importance of the physical properties of simple bentonite particles and binary mixtures in order to understand the fluidization operating parameters. The fluidization is necessary to achieve a completely mixed bed and to reduce or eliminate partial or total segregation of the particles, which can affect the gas-solid contact. The dynamic parameters were determined at the moment of incipient fluidization to prevent the action of inter-particle forces that exist in the case of small particles. Besides this aspect, the use of bentonite particles in the fluidization process is recommended due to their high specific surface areas, making them suitable for forming a binary fluidized bed for future research in adsorption processes.

To complete this study, empirical equations were applied for estimation of the minimum fluidization velocity of simple bentonite particules and binary mixture using regression analysis.

## MATERIALS AND METHODS

The experimental setup used in this study is presented in Figure 2. The fluidization column is constructed from a transparent Pyrex tube with an internal diameter of D =  $5 \cdot 10^{-2}$  m, a height column of H =  $40 \cdot 10^{-2}$  m, and a cross-sectional area of A =  $19.62 \cdot 10^{-4}$  m². Dried and filtered compressed air was supplied to the particle bed through a porous gas distributor plate. The air flow rate was measured using a Shorate 1355 flowmeter (0 -  $60 \cdot L \cdot min^{-1}$  air, p = 2 bar, T =  $20^{\circ}C$ ) and a Broks GT 1024 flowmeter

St. Cerc. St. CICBIA 2025 26 (1)

 $(0-280 \text{ L} \cdot \text{min air}^{-1}, p=2 \text{ bar}, T=20^{\circ}\text{C})$ . The particles used in these fluidization tests are bentonite clay. Bentonite is natural clay composed of about 50 - 70 % montmorillonite, with the remainder being impurities such as feldspar, mica, quartz, cristobalite, coarse sand etc. [44-46].

The bentonite particles are arranged in the column in a pseudo-homogeneous configuration [16, 47]. The pressure drop across the ascending bentonite particle bed was measured using a digital manometer Keller PD 33 H via a transducer Converter K-107 Keller connected to a computer.

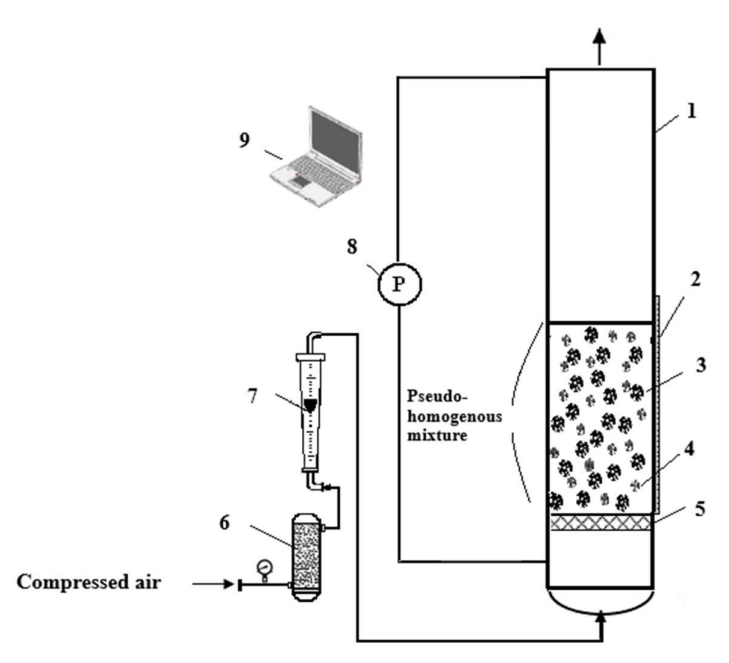


Figure 2. Experimental set-up

1 – fluidization column; 2 – graduated scale; 3 – sodium bentonite particles; 4 – calcium bentonite particles; 5 – porous plate; 6 – air desiccators column; 7 – flowmeter; 8 – differential manometer; 9 – computer.

Two types of bentonite particles were used in a pseudo-homogeneous configuration: sodium bentonite (*NaBent*) [48] and calcium bentonite (*CaBent*) [49]. The specific surface area of sodium bentonite is 16.88 m<sup>2</sup>·g<sup>-1</sup>, and that of calcium bentonite is 46.52 m<sup>2</sup>·g<sup>-1</sup>, as reported in a previous publication [50].

The bentonite particles were initially in powder form. To obtain particles with high granulometry and sphericity, they were agglomerated with distilled water in a ratio of 1: 3, dried at 110 °C, and manually triturated. The particles were then introduced into the fluidization column to form a granular bed, and the bed height ( $H_0$ ) was measured using a graduated scale fixed to the fluidization column.

The physical properties of the particles used in the fluidization tests of the monocomponent bed, such as particle shape  $(\Psi)$ , average particle diameter  $(\overline{d}_p)$ , and average particle density  $(\overline{\rho}_p)$ , were experimentally determined.

The particle shape was determined by analyzing bentonite images taken with a Kruss optical microscope equipped with a Topica TP 100 digital camera. The geometry of the

2D images was then calculated. Sodium and calcium bentonite particles have irregular and asymmetric shapes [51], falling into the spheroid category [2]. These materials are non-spherical particles, and the average diameter of bentonite particles ( $\overline{d}_p$ ) is defined as the equivalent diameter of a particle with the same volume. As an approximation, the average particle diameter can be considered from the geometric mean of two consecutive sieve openings without introducing significant errors [52, 53].

The average particle diameter of bentonite  $(\overline{d}_p)$  was determined using the classic dry sieving method [54]. The determination of the average particle diameter was performed with a Retsh Ficher AS 200 sieving device, equipped with standardized sieves vertically placed in decreasing mesh size order, at amplitude of 60 vibrations for 7 minutes. Two size classes were obtained:  $\overline{d}_p = 0.75 \cdot 10^{-3}$  m and  $\overline{d}_p = 1.5 \cdot 10^{-3}$  m [18].

The average particle density  $(\overline{\rho}_p)$  was determined by the volumetric method using a graduated cylinder. Cyclohexane was used as the liquid for measuring the average bulk density of the clay particles instead of water, due to the swelling properties of clays [50]. The results obtained are presented in Table 1.

**Table 1.** Physical properties of bentonite particles

Bentonite particles	Particles shape, Ψ (-)	Average particle diameter, $\overline{d}_p$ [10-3, m]	Average particle  density,   [kg·m-3]	Geldart group
NaBent	0.74	0.75	2026	В
	0.70	1.50	2394	D
CaBent	0.85	0.75	1768	В
	0.81	1.50	1935	D

Depending on Geldart's dimensional-dynamic classification, the type of fluidization for a mono-component bed can be identified by knowing the average particle diameter ( $\overline{d}_p$ ) and the average particle density ( $\overline{\rho}_p$ ). The studied materials can be classified into two groups: Group B, which contains most particles with an average diameter of  $\overline{d}_p = 0.75 \cdot 10^{-3} m$ , and Group D, which contains particles with a larger average diameter of  $\overline{d}_p = 1.5 \cdot 10^{-3} m$ . Although the two types of particles will behave differently during fluidization, the transition point from the fixed bed to the bubbling regime is determined by the minimum fluidization velocity in both cases.

## Mixture Data

Using previous experimental results obtained from the classical fluidization of simple particles, particles with the same diameter but different densities were selected to achieve a pseudo-homogeneous configuration. These particles have similar minimum fluidization velocities and will form a binary mixture. The binary mixture used in the experimental study consists of sodium and calcium bentonite particles, referred to as mixture A and mixture B, respectively. The physical properties of these mixtures are presented in Table 2.

**Table 2.** Physical properties of binary mixture

Mixture	Mass fraction $(x_{NaBent})$	Average mixture diameter, $\overline{d}_{p,mix}$ [10 <sup>-3</sup> , m]	Average mixture density,	Volumetric fraction $(x_{v,NaBent})$	Volumetric average mixture diameter, $\overline{d}_{v,mix}$ [10-3, m]	$\frac{-}{\rho_{p,NaBent}}$ $\frac{-}{\rho_{p,CaBent}}$
A	0.57	0.75	1870.42	0.5377	0.59	1.15
В	0.57	1.5	2108.86	0.5186	1.12	1.24

Each of the two mixtures in a pseudo-homogeneous configuration was sieved to measure and weigh the mass fraction of sodium bentonite ( $x_{NaBent}$ ). To determine the minimum fluidization velocity for the mixture bed ( $U_{mf,mix}$ ), the physical properties presented in Table 2 were calculated: average particle diameter ( $\overline{d}_{p,mix}$ ) [41], average particle density ( $\overline{\rho}_{p,mix}$ ) [42], volumetric fraction for sodium bentonite particles using equation (5), and volumetric average mixture diameter using equation (6). The same table also reports the density ratio of the components to investigate the role of density differences in binary fluidization.

In the classical fluidization of a mixture consisting of sodium and calcium bentonite, where the particles have the same diameter but different densities, the mixture with higher density particles  $(\overline{d}_{p,mix} = 1.5 \cdot 10^{-3} \, m \text{ and } \overline{\rho}_{p,mix} = 2108.86 \, kg \cdot m^{-3})$  represents the "Jetsam" particles, which will settle at the bottom of the fluidization column. Conversely, particles  $(\overline{d}_{p,mix} = 0.75 \cdot 10^{-3} m)$ mixture lower density the with  $\overline{\rho}_{p,mix} = 1870.42 \, kg \cdot m^{-3}$ ) represents the "Flotsam" particles, which will remain in the upper part of the bed. After fluidization, it can be expected that a completely segregated bed will be obtained. The measurements showed that the mixture of particles passes through three fluidization regimes: fixed bed, well-mixed bed, and fully segregated bed. The fluidization tests in a pseudo-homogeneous configuration were carried out with bed weights (G) of 200 g for sodium bentonite (NaBent) and 150 g for calcium bentonite (CaBent), corresponding to bed height-to-diameter ratios ( $H_0/D$ ) nearly equal to 2. The mass fraction of NaBent particles ( $x_{NaBent}$ ) was 0.57. At the beginning of the fluidization experiment, the binary system was charged into the column in a fixed bed with wellmixed particles in a pseudo-homogeneous configuration.

The objectives of these tests were to determine the experimental values at increasing flow rates  $(G_v)$  for the two binary mixtures and to measure their mixing state at fluidizing velocities near the minimum and complete velocities, following the fluidization diagram  $(\Delta P - U_g)$  for a mixing or segregating bed. The behavior of particles in a pseudo-homogeneous configuration was also visually observed through the transparent fluidization column.

## RESULTS AND DISCUSSION

Dynamic parameters in classical fluidization of simple particles (NaBent and CaBent) The experimental tests on the dynamics of simple particle beds involved measuring the volumetric air flow rate  $(G_v)$  from 0 to 50 L min<sup>-1</sup> for NaBent particles with  $\overline{d}_p = 0.75 \cdot 10^{-3} \, m$  and from 0 to 140 L min<sup>-1</sup> for CaBent particles  $\overline{d}_p = 1.5 \cdot 10^{-3} \, m$ . To determine the fluidization regime for this gas-solid system, the Froude number [2] was calculated using equation (1), indicating that all bentonite particles exhibit particulate fluidization behavior.

The parameters varied in this particulate fluidization study included the average particle diameter  $(\overline{d}_p)$  and the initial height of the fixed bed  $(H_0)$ . Table 3 presents the experimental values at increasing flow rates  $(G_v)$  for the minimum pressure drop  $(\Delta P_{min, exp.})$  and the minimum fluidization velocity  $(U_{mf, exp.})$  according to the incipient bed fluidization.

The fixed bed porosity ( $\varepsilon_0$ ) [15, 16], the minimum pressure drop ( $\Delta P_{min, calc.}$ ) using empirical equation (2), the Reynolds number using dimensionless equation (3), and the minimum fluidization velocity ( $U_{mf, calc.}$ ) using equation (4) were also calculated.

**Table 3.** Dynamic parameters at incipient fluidization for simple particles

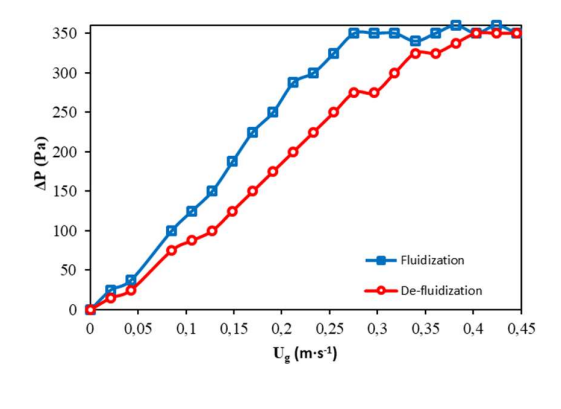
		$(10^{-3}, \mathbf{m})$	H <sub>0</sub>		Experimental		Calculated			
N <sup>0</sup> tests	Bentonite particles		$l_p$ (10-2.	ΔP <sub>min</sub> (Pa)	$U_{mf}$ $(m \cdot s^{-1})$	ε <sub>0</sub> (-)	ΔP <sub>min</sub> (Pa)	Remf	$U_{mf}$ $(m \cdot s^{-1})$	
1.			2.5	287.5	0.31	0.459	268.64	15.71	0.298	
2.			5	440	0.33	0.506	491.59			
3.		0.75	7.5	575	0.33	0.503	740.37			
4.		0.73	10	837.5	0.33	0.507	979.22			
5.			12.5	1062.5	0.33	0.503	1236.43			
6.	NaBent		15	1350	0.33	0.498	1519.47			
7.	мавет	1.50	2.5	200	0.59	0.536	272.87	82.40	0.781	
8.			5	430	0.67	0.579	495.27			
9.			7.5	575	0.67	0.575	749.94			
10.			10	875	0.76	0.573	1002.27			
11.			12.5	1150	0.67	0.595	1191.23			
12.			15	1287.5	0.67	0.577	1492.85			
13.		0.75	2.5	187.5	0.16	0.547	196.12	13.99	0.265	
14.			5	362.5	0.23	0.546	393.46			
15.			7.5	425	0.25	0.564	566.91			
16.		0.75	10	637.5	0.27	0.572	742.21			
17.		ConDonat	12.5	825	0.31	0.579	911.71			
18.	CaBent		15	1037.5	0.27	0.561	1142.51			
19.		1.50	2.5	175	0.42	0.582	198.24	71.71		
20.			5	275	0.50	0.580	398.78			
21.			7.5	450	0.59	0.620	540.58			
22.			10	738.5	0.59	0.598	762.59			
23.			12.5	800	0.67	0.620	901.48			
24.			15	1087.5	0.76	0.616	1091.77			

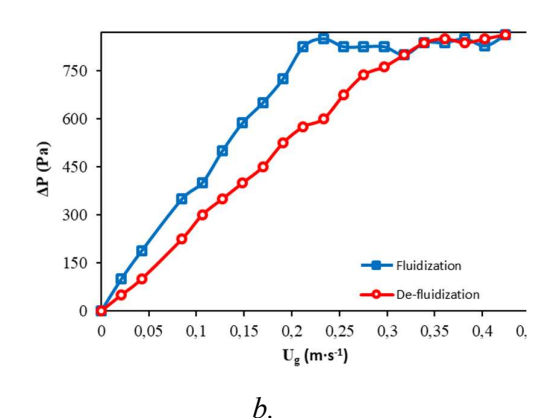
Because the bentonite particles used in the experiments belong to Groups B and D, they exhibit high bed porosity in the fixed bed due to the increase in average particle diameter  $(\overline{d}_p)$  and bed height  $(H_0)$ . These bentonite particles do not show homogeneous expansion when are fluidized, and the fixed bed porosity  $(\varepsilon_0)$  is always considered equal to the bed porosity at incipient fluidization  $(\varepsilon_{mf})$  [55].

It was found that the experimental values for the minimum pressure drop ( $\Delta P_{min, exp.}$ ) show a deviation from the theoretical values in the range of -4% to -37% for sodium bentonite particles and -0.4% to -34% for calcium bentonite particles. Table 3 provides the possibility to predict the minimum fluidization velocity ( $U_{mf}$ ) for a mono-component bed, calculated using the most popular equation (4) based on the work of Wen and Yu in the laminar flow region [17, 19, 56]. The agreement with all experimental data is acceptable, with the lowest error being related to bentonite particles with  $\overline{d}_p = 0.75 \cdot 10^{-3} m$ , where the average error is +6.87% for *NaBent* and -6.85% for *CaBent*, and for particles with  $\overline{d}_p = 1.5 \cdot 10^{-3} m$ , where the average error is -16.04% for *NaBent* and -15.64% for *CaBent* 

The establishment of dynamic parameters in a mono-component bed consisting of bentonite particles was achieved by measuring the pressure drop  $(\Delta P)$  and supplementing these measurements with visual observations of the particle bed height  $(H_0)$  for each value of the volumetric air flow rate  $(G_v)$ . Experimental values for the  $\Delta P_{min}$  and  $U_{mf}$  were determined from specific diagrams that characterize the fluidization regimes, representing the evolution of the pressure drop  $(\Delta P)$  in the bed (measured with a digital manometer) as a function of  $U_g$ .

The hysteresis phenomenon was continuously monitored by reading the pressure drop value during both increasing (fluidization) and decreasing (de-fluidization) air flow, as shown in Figures 3 and 4. Fluidization diagrams ( $\Delta P - U_g$ ) are presented for bentonite particles (*NaBent* and *CaBent*) with an average particle diameter of  $0.75 \cdot 10^{-3} m$  at different geometric ratios ( $H_0/D$ ).





а.

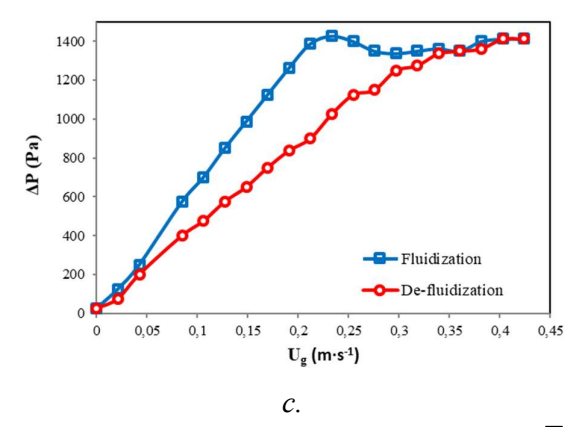


**Figure 3.** Fluidization diagrams for NaBent particles with  $\overline{d}_p = 0.75 \cdot 10^{-3} \, m$  $H_0/D = 1$ ; b.  $H_0/D = 2$ ; c.  $H_0/D = 3$ 

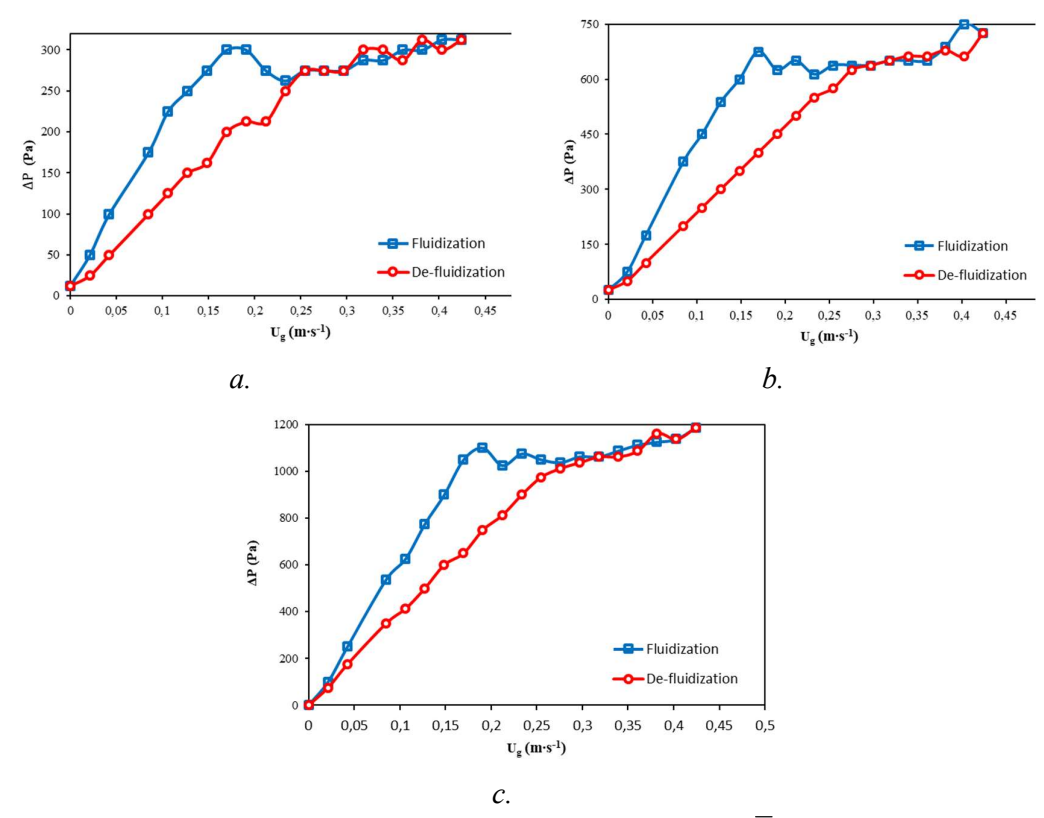


**Figure 4.** Fluidization diagrams for CaBent particles with  $\overline{d}_p = 0.75 \cdot 10^{-3} m$  $H_0/D = 1$ ; b.  $H_0/D = 2$ ; c.  $H_0/D = 3$ 

The fluidization regimes were determined by referencing the  $U_{mf}$  at different geometric ratios  $(H_0/D)$ , depending on the average particle diameter  $(\overline{d}_p = 0.75 \cdot 10^{-3} m)$ . Analyzing the  $(\Delta P - U_g)$  curves shown in the fluidization diagrams for bentonite particles, in a fixed bed, the particles remain stationary at low gas velocities, slipping between the stationary

St. Cerc. St. CICBIA 2025 26 (1)

particles, and the pressure drop is smaller than the bed weight ( $\Delta P < G$ ). At the  $U_{mf}$ , the bentonite particles are suspended, having a certain degree of freedom to move around their fixed positions, and the pressure drop equals the apparent bed weight per unit cross-section of the fluidization column ( $\Delta P = G$ ). Small gas bubbles appear in the bed at this stage.

At high gas velocities, turbulent fluidization occurs, and large gas bubbles disrupt the bed particles. To avoid this inconvenience, it is necessary to add other particles with different physical properties. Upon de-fluidization, the bed exhibits the same behavior in the opposite direction. At the end, the particles settle again due to gravity, forming a fixed bed depending on particle shape, average particle diameter, and average particle density. From the classical fluidization tests of simple particles (sodium and calcium bentonite), particles that show similar values of the  $U_{mf}$  at incipient fluidization were selected to create the binary mixture.

## Dynamic parameters in classical fluidization of two types of particles in pseudohomogeneous configuration

All the experiments in this study were performed in the same fluidization column, under the same conditions as the simple particle fluidization presented in Figure 2. The constant parameters are the bed weights (G), geometric bed ratios  $(H_0/D)$ , and the mass fraction of sodium bentonite particles  $(x_{NaBent})$ .

The variable parameters include the minimum fluidization velocities specific to the binary mixture, the pressure drop at incipient fluidization ( $\Delta P_{min, mix}$ ), and the pressure drop at the moment of fluidization ( $\Delta P_{mf, mix}$ ). The dynamic parameters at incipient fluidization for the binary mixture are presented in Table 4.

**Table 4.** Dynamic parameters at the incipient fluidization for bentonite particle in pseudo-homogeneous configuration

	Experimental					Calculated
Mixture	U <sub>if</sub> [m·s <sup>-1</sup> ]	$U_{mf, mix} = [\mathbf{m} \cdot \mathbf{s}^{-1}]$	$U_{tf}$ $[\mathbf{m}\cdot\mathbf{s}^{-1}]$	$\Delta P_{min, mix}$ [Pa]	$\begin{array}{c c} \Delta P_{mf, mix} \\ [Pa] \end{array}$	$\mathbf{U}_{\mathbf{mf,\ mix}} \ [\mathbf{m} \cdot \mathbf{s}^{-1}]$
A	0.296	0.360	0.445	1725	1635	0.292
В	0.678	0.848	1.017	1426	1425	0.652

The values presented in Table 4 were obtained from the  $(\Delta P - U_g)$  fluidization curves, identifying three fluidization velocities based on the gas flow rate:  $U_{if}$  represents the initial fluidization velocity,  $U_{mf, mix}$  represents the minimum fluidization velocity for well-mixed particles, and  $U_{tf}$  represents the total fluidization velocity at which all the particles begin to fluidize with gas bubbles [57].

The experimental values of the minimum fluidization velocity for mixtures A and B are compared with the calculated values using the empirical correlation for  $U_{mf.\ mix}$  proposed by Chiba for a completely segregated bed with different diameters and/or densities [28], using equation (7).

To calculate the minimum fluidization velocity for binary particles in a pseudo-homogeneous configuration, it is necessary to know the minimum fluidization velocity values for simple particles previously determined. The minimum fluidization velocities of bentonite particles determined in preliminary experiments are as follows: for *NaBent* particles,  $U_{mf}$  is 0.33 m·s<sup>-1</sup>, and for *CaBent* particles,  $U_{mf}$  is 0.27 m·s<sup>-1</sup> with an average

particle diameter of  $\overline{d}_p = 0.75 \cdot 10^{-3} \, m$ . For *NaBent* particles,  $U_{mf}$  is  $0.76 \, \text{m} \cdot \text{s}^{-1}$ , and for *CaBent* particles,  $U_{mf}$  is  $0.59 \, \text{m} \cdot \text{s}^{-1}$  with an average particle diameter of  $\overline{d}_p = 1.5 \cdot 10^{-3} \, m$ . After calculating the minimum fluidization velocity for binary particles, mixture A shows an average error of + 6.71 % (Table 4), which is lower than the average error of + 19.52 % for mixture B. This is due to the increase in particle diameter in the mixture, which increases the influence of the wall effect, making it difficult to fluidize and estimate the experimental values.

When a gas flow  $(G_v)$  passes through a fixed bed of bentonite particles in the laminar flow region, the pressure drop at incipient fluidization  $(\Delta P_{min, mix})$  inversely varies with the particle diameter. These phenomena are due to the increase in frictional force between particles and gas present in mixture A. The value for the pressure drop at incipient fluidization  $(\Delta P_{min, mix})$  is almost the same as that for well-mixed particles  $(\Delta P_{min, mf})$  in the case of mixture B, because the particles have a larger diameter, and their movement is slowed down.

The fluidization diagrams ( $\Delta P$  -  $U_g$ ) for particle mixtures with  $x_{NaBent} = 0.57$  and  $H_0/D = 2$  are presented in Figure 5.

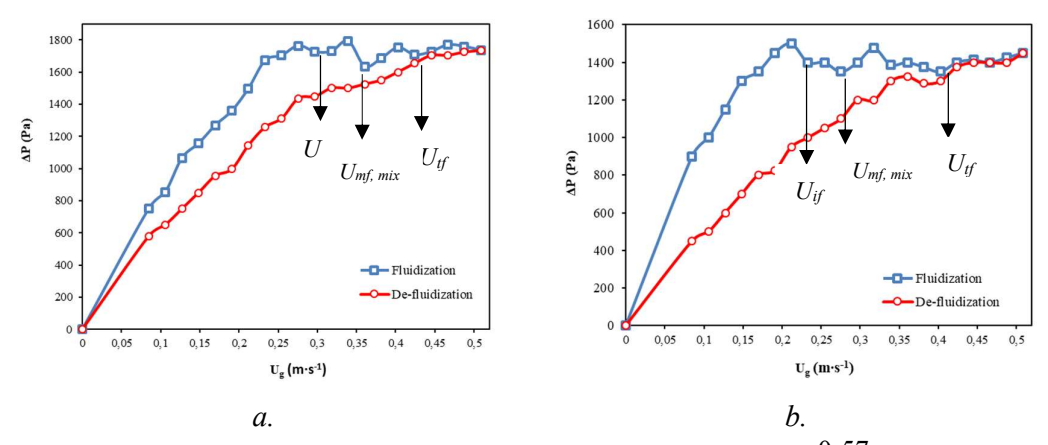


**Figure 5.** Fluidization diagrams for particle mixture with  $x_{NaBent} = 0.57$  and  $H_0/D = 2$  a. Mixture A; b. Mixture B

As observed in Figure 5, when the  $U_g$  is gradually increased, different patterns of pressure drop growth are obtained. When transitioning from a fixed bed to a fluidized bed in this configuration, three points or discontinuities corresponding to the values of  $U_{if}$ ,  $U_{mf, mix}$  and  $U_{tf}$  appear in the respective graphs.

Understanding the dynamic parameters is important because the high pressure drop associated with small diameter particles in mixture A with  $\overline{d}_p = 0.75 \cdot 10^{-3} m$  compromises the cost of the fluidization process [45].

## Comparison between experimental data and values obtained from empirical model for minimum fluidization velocity

Since the equations did not acceptably approximate the experimental values of minimum fluidization velocity for NaBent and CaBent particles, as well as for the pseudo-homogeneous configuration, other mathematical equations will be proposed. By applying regression analysis to the experimental data, an empirical equation is found for  $U_{mf}$  and

 $U_{mf,mix}$ , depending on the average particle diameter  $(\overline{d}_p)$ , the geometric ratio  $(H_0/D)$ , or the density ratio. The empirical equations for simple particles and mixture particles are presented in Table 5.

Particles	Empirical equation	Average error [%]
NaBent	$U_{mf} = 2,67 \cdot 10^{-8} \cdot \overline{d}_{p}^{0,42} \cdot \left(\frac{H_{0}}{D}\right)^{0,08} \cdot \left(\frac{\overline{\rho}_{p} - \rho_{g}}{\eta_{g}} \cdot g\right)^{0,779}$	7
CaBent	$U_{mf} = 5.37 \cdot 10^{-3} \cdot \overline{d}_{p}^{1.227} \cdot \left(\frac{H_{0}}{D}\right)^{0.145} \cdot \left(\frac{\overline{\rho}_{p}}{\rho_{g}}\right)^{0.618}$	10
Mixure	$U_{mf,mix} = 6,6507 \cdot \overline{d}_{p}^{1.8468} \cdot \left(\frac{H_{0}}{D}\right)^{-1.4457}$	0

**Table 5.** Empirical equations for estimation of the minimum fluidization velocity of simple and mixture particles

The equations correctly estimate the experimental values. The average error for the minimum fluidization velocity is 7 % for sodium bentonite particles, 10 % for calcium bentonite particles, and 0 % for mixture particles, as shown in the table.

## CONCLUSIONS

The experimental investigation of the dynamic parameters in particulate fluidization shows that the bed behavior of *NaBent* and *CaBent* particles is influenced by average diameter and average density of the particles. Bentonite particles with  $\overline{d}_p = 0.75 \cdot 10^{-3} m$  belong to Group B and bentonite particles with  $\overline{d}_p = 1.5 \cdot 10^{-3} m$  belong to Group D. The empirical equation for  $U_{mf}$  obtained for the main operating parameters approximates the experimental data with an acceptable error.

Analyzing the initial investigation for the simple particles, the experimental results are crucial for selecting particles with approximate values for minimum fluidization velocities to achieve a pseudo-homogeneous configuration. The binary mixture is strongly influenced by the internal composition profile in the fixed bed, which is associated with the variation in pressure drop. This variation significantly affects the onset of fluidization and component segregation, with the "Jetsam" particles being the NaBent particles. The dynamic parameters are important because the high  $\Delta P$  associated with small diameter particles would eventually lead to high energy costs, compromising the fluidization process.

Based on dimensional analysis and experimentation, equations are proposed to estimate the minimum fluidization velocity of simple and mixture particles. These equations have an error rate of under 10 %. This approach is beneficial for using cylindrical columns to fluidize bed particle mixtures with applications in different industries.

Besides its potential application in the development of multi-functional fluidization columns involving simultaneous reaction and adsorption, binary particle fluidization can

help modify the basic dynamic characteristics of a fluidized bed. Adding particles with different physical properties than the initial solid phase of the fluidized bed is a good solution. However, in process industries, gas-solid contacting involving small particles in a mixture poses a major challenge, whether implemented in a fixed bed or a fluidized bed. A large specific surface area ensures high heat and mass transfer rates and better utilization of adsorbent or catalyst particles, but bubbling appears in the bed with local turbulence and slug flow, leading to segregation phenomena.

In the future, alternatives can be found to stabilize the bed during the fluidization process by applying external forces, such as an electro-magnetic field, to fix the particles bed consisting of *NaBent* and/or *CaBent* particles within the magnetic bed.

## **ACKNOWLEDGEMENTS**

These dynamics studies were carried out using the fluidization installation included in the equipment of "Génie chimique et biochimique" laboratory, from the "Clermont Auvergne" University, France. The authors wish to express their appreciation to Mr. Prof. Gholamreza Djelveh and the entire team for their availability and technical and scientific effort.

### LIST OF SYMBOLS

A	cross-section fluidization column	$[m^2]$
$\overline{d}_{p}$	average particle diameter	[m]
$\overline{d}_{p,mix}$	average particle diameter mixture	[m]
$\overline{d}_{v,mix}$	volumetric particle diameter mixture	[m]
g	gravity acceleration	$[m \cdot s^{-2}]$
G	bed weight	[kg]
$G_{v}$	volumetric flow	$[L \cdot min^{-1}]$
D	column diameter	[m]
$H_0$	fixed bed height	[m]
$H_{mix}$	mixed particles height	[m]
$H_{Jetsam}$	packet or "Jetsam" height	[m]
$U_b$	minimum bubbling velocity	$[\mathbf{m} \cdot \mathbf{s}^{-1}]$
$U_g$	gas (air) velocity	$[\mathbf{m} \cdot \mathbf{s}^{-1}]$
$U_{mf}$	minimum fluidization velocity	$[\mathbf{m} \cdot \mathbf{s}^{-1}]$
$U_{if}$	initial fluidization velocity	[m·s <sup>-1</sup> ]
$U_{mf,mix}$	minimum fluidization velocity of the mixture	$[\mathbf{m} \cdot \mathbf{s}^{-1}]$
$U_{t\!f}$	total fluidization velocity	$[\mathbf{m} \cdot \mathbf{s}^{-1}]$
x	mass fraction	[-]
$x_{v}$	volumetric fraction	[-]

gas density

average particle density

Greek letters

 $[kg \cdot m^{-3}]$ 

 $[kg \cdot m^{-3}]$ 

$\overline{ ho}_{_{p,mix}}$	average particles density mixture	[kg·m <sup>-3</sup> ]
$\Delta P_{min}$	minimum pressure drop	[Pa]
Ψ	particle shape	[-]
$\mathcal{E}_{0}$	fixed bed porosity	[-]
$\eta_g$	gas viscosity	[Pa·s]
Criteria		
Fr	Froude	[-]
Re	Reynolds	[-]
Ar	Archimedes	[-]
Subscrip	ts	
J	"Jetsam" particles	
F	"Flotsam" particles	
calc.	value determined by equations	
exp.	value determined practically by experiment	
mix	mixture of the particles	

### REFERENCES

- 1. Khawaja, H.: CFD-DEM Simulation of Minimum Fluidisation Velocity in Two Phase Medium, *The International Journal of Multiphysics*, **2011**, **5** (2), 89-100;
- Gilbertson, M.A., Eames, I.: The Influence of Particle Size on the Flow of Fluidised Powders, Powder Technology, 2003, 131 (2-3), 197-205;
- 3. Shi, M.H., Zhao, Y.B., Liu, Z.L.: Study on Boiling Heat Transfer in Liquid Saturated Particle Bed and Fluidized Bed, *International Journal of Heat and Mass Transfer*, **2003**, <u>46</u> (24), 4695-4702;
- 4. Zhang, W.: A Review of Techniques for the Process Intensification of Fluidized Bed Reactors, *Chinese Journal of Chemical Engineering*, **2009**, <u>17</u> (4), 688-702;
- 5. Turchiuli, C.: Fluidization in Food Powder Production in: *Handbook of Food Powders: Processes and Properties*, **2013**, <u>255</u>, 178-199;
- 6. Lettieri, P., Macrì, D.: Effect of Process Conditions on Fluidization, *KONA Powder and Particle Journal*, **2016**, <u>33</u>, 86-108;
- 7. Moșneguțu, E., Nedeff, V., Bârsan, Rusu, D.: The Influence o Air Velocity on the Behavior of a Solid Particle Displacement in a Vertical Path, *Scientific Study and Research: Chemistry and Chemical Engineering, Biotechnology, Food Industry*, **2018**, **19** (4), 431-441;
- 8. Lim, K.S., Zhu, J.X., Grace, J.R., Hydrodynamics of Gas-Solid Fluidization, *International Journal of Multiphase Flow*, **1995**, **21**, 141-193;
- 9. Mawatari, Y., Kawai, A., Yuji T., Noda, K.: Minimum Bubbling Velocity and Homogeneous Fluidization Region under Reduced Pressure for Group-A Powders, *Particle Technology and Fluidization*, **2004**, <u>37</u> (1), 89-94;
- Han, Z., Yue, J., Geng, S., Hu, D., Liu, X., Suleiman, S.B., Cui, Y., Bai, D., Xu, G.: State-of-the-Art Hydrodynamics of Gas-Solid Micro Fluidized Beds, *Chemical Engineering Science*, 2021, 232, 116345;
- 11. Zhang, Y., Goh, K.-L., Ng, Y.L., Chow, Y., Wang, S., Zivkovic, V.: Process Intensification in Micro-Fluidized Bed Systems: A review, *Chemical Engineering and Processing Process Intensification*, **2021**, <u>164</u>, 108397;
- 12. Singh, R.K., Roy, G.K.: Prediction of Minimum Bubbling Velocity, Fluidization Index and Range of Particulate Fluidization for Gas–Solid Fluidization in Cylindrical and Non-Cylindrical Beds, *Powder Technology*, **2005**, **159** (3), 168-172;
- 13. Li, S., Zhang, Y., Wang, W., Wang, H.: Comparative Analysis of Particle Density Effects on Initial Fluidization in Gas-Solid Fluidized Beds, *Chemical Engineering Journal*, **2023**, <u>477</u>, 146966;

- 14. Gros, F., Ursu, A.-V., Djelveh, G., Jinescu, C., Nistor, I. D., Jinescu, G.: Aspects of Structure of Fluidized Bed Mixture of Magnetic and Nonmagnetic Particles in Magnetic Field, *Revista de Chimie*, **2010**, <u>6</u> (6), 590-594;
- Muntianu, G., Ursu, A.-V., Djelveh, G., Isopencu, G., Mareş, A.-M., Nistor, I.D., Jinescu, C.V.: Dynamic Parameters for Mixtures of Pillared Clay-Magnetic Particles in Fluidized Bed in Coaxial Magnetic Field, Revista de Chimie, 2014, 65 (9), 1077-1085;
- Timsina, R., Thapa, R.K., Moldestad, B.M.E.: Eikeland, M.S., Effect of Particle Size on Flow Behavior in Fluidized Beds, *International Journal of Energy Production and Management*, 2019, 4 (4), 287-297;
- Muntianu, G., Platon, N., Arus, V.A., Rosu, A.M., Nistor, D.I., Jinescu, G.: Hydrodynamic Study of Clay Particles in Fluidized Bed, *Journal of Engineering Studies and Research*, 2013, 19 (2), 70-75;
- 18. Anantharaman, A., Cocco, R.A., Chew, J.W.: Evaluation of Correlations for Minimum Fluidization Velocity (Umf) in Gas-Solid Fluidization, *Powder Technology*, **2018**, <u>323</u>, 454-485;
- 19. Geldart, D.: Types of Gas Fluidization, *Powder Technology*, **1973**, <u>7</u>, 285-292;
- Shaul, S., Rabinovich, E., Kalman, H.: Typical Fluidization Characteristics for Geldart's Classification Groups, *Particulate Science and Technology*, 2014, 32 (2), 197-205;
- Xu, C., Cheng, Y., Zhu, J.: Fluidization of Fine Particles in a Sound Field and Identification of Group C/A Particles using Acoustic Waves, *Powder Technology*, 2006, 161 (3), 227-234;
- 22. Ye, M., van der Hoef, M.A., Kuipers, J.A.M.: The Effects of Particle and Gas Properties on the Fluidization of Geldart A Particles, *Chemical Engineering Science*, **2005**, **60** (16), 4567-4580;
- Du, H., Zhou, Y., Zhao, D., Shao, Y., Zhu, J.: Fluidization Stability vs. Powder History of Geldart Group C<sup>+</sup> Particles, *Powder Technology*, 2021, 384, 423-430;
- 24. Mareş, A.M., Isopencu, G., Jinescu, C.: Aspects Concerning the Drying of Granular Biomaterials with Intensive Techniques. Dynamics of Modified Fluidized Bed in the Presence of Inert Particles, *Revista de Chimie*, **2008**, **59** (1), 79-87;
- Isopencu, G., Mares, A.M., Jinescu, G.: Interparticular Forces in Powdery Materials Beds, University Politehnica of Bucharest Scientific Bulletin Series B - Chemistry and Materials Science, 2007, 69 (3), 27-34;
- Huilin, L., Yunhua, Z., Ding, J., Gidaspow, D., Wei, L.: Investigation of Mixing/Segregation of Mixture Particles in Gas-Solid Fluidized Beds, *Chemical Engineering Science*, 2007, 62 (1-2), 301-317.
- Rowe P.N., Nienow A.W.: Particle Mixing and Segregation in Gas Fluidised Beds. A review, *Powder Technology*, 1976, 15(2), 141-147;
- Chiba, S., Chiba, T., Nienow, A.W., Kobayashi, H.: The Minimum Fiuidisation Velocity Bed Expansion and Pressure-Drop Profile of Binary Particle Mixtures, *Powder Technology*, 1979, <u>22</u> (2), 255-269;
- Wu, G., Yu, B., Guan, Y., Wu, X., Zhang, K., Li, Y.: Mixing Characteristics of Binary Mixture with Biomass in a Gas-Solid Rectangular Fluidized Bed, *Energies*, 2019, <u>12</u> (10), 2011, https://doi.org/10.3390/en12102011
- 30. Di Maio, F.P., Di Renzo, A., Vivacqua, V.: A Particle Segregation Model for Gas-Fluidization of Binary Mixtures, *Powder Technology*, **2012**, <u>226</u>, 180-188;
- 31. Lv, B., Luo, Z., Fu, Y., Zhang, B., Qin, X., Zhu, X.: Particle Mixing Behavior of Fine Coal in Density Control of Gas-Solid Separation Fluidized Bed, *Particuology*, **2020**, **50**, 76-87;
- 32. Turrado, S., Fernandez, J.R., Abanades, J.C.: Investigation of the Segregation of Binary Mixtures with Iron-Based Particles in a Bubbling Fluidized Bed, *ACS Omega*, **2019**, **4**, 9065–9073;
- Formisani, B., Girimonte, R., Longo, T.: The Fluidization Process of Binary Mixtures of Solids: Development of the Approach Based on the Fluidization Velocity Interval, *Powder Technology*, 2008, 185, 97–10;
- 34. Emiola-Sadiq, T., Wang, J., Zhang, L., Dalai, A.: Mixing and Segregation of Binary Mixtures of Biomass and Silica sand in a Fluidized Bed, *Particuology*, **2021**, **58**, 58-73;
- 35. Formisani, B., Girimonte, R., Vivacqua, V.: Fluidization of Mixtures of Two Solids Differing in Density or Size, *AIChE Journal*, **2011**, **57** (9), 2325-2333;
- Girimonte, R., Formisani, B., Vivacqua, V.: The Relationship Between Fluidization Velocity and Segregation in Two-Component Gas Fluidized Beds: Density or Size-Segregating Mixtures, Chemical Engineering Journal, 2018, 335, 63-73;

- 37. Formisani, B., Girimonte, R., Vivacqua, V.: Fluidization of Mixtures of Two Solids: A Unified Model of the Transition to the Fluidized State, **2013**, **59** (3), 729-735;
- 38. Formisani, B., Girimonte, R., Vivacqua, V.: The Interaction Between Mixture Components in the Mechanism of Binary Fluidization, *Powder Technology*, **2014**, **266**, 228-235;
- 39. Formisani, B., Girimonte, R., Longo, T.: The Fluidization Process of Binary Mixtures of Solids: Development of the Approach Based on the Fluidization Velocity Interval, *Powder Technology*, **2008**, **185** (2), 97-108;
- Fu, Z., Zhu, J., Barghi, S., Zhao, Y., Luo, Z., Duan, C.: Minimum Fluidization Velocity of Binary Mixtures of Medium Particles in the Air Dense Medium Fluidized Bed, *Chemical Engineering Science*, 2019, 207, 194-201;
- Agu, C.E., Pfeifer, C., Moldesta, B.M.E.: Prediction of Void Fraction and Minimum Fluidization Velocity of a Binary Mixture of Particles: Bed Material and Fuel Particles, *Powder Technology*, 2019, 349, 99-107;
- 42. Cáceres-Martínez, L.E., Guío-Pérez, D.C., Rincón-Prat, S.L.: Significance of the Particle Physical Properties and the Geldart Group in the Use of Correlations for the Prediction of Minimum Fluidization Velocity of Biomass–Sand Binary Mixtures, *Biomass conversion and biorefinery*, **2023**, <u>13</u> (2), 935-951;
- 43. Mirilă, D.C., Pîrvan, M.Ş., Roşu, A.M., Zichil, V., Nistor, I.D.: Activated Adsorption on Clay of Micropollutants from Paper Printing Industry, *Scientific Study and Research-Chemistry and Chemical Engineering Biotechnology Food Industry*, **2018**, **19** (1), 063-072;
- 44. Li, Z., Kobayashi, N., Nishimura, A., Hasatani, M.: A Method to Predict the Minimum Fluidization Velocity of Binary Mixtures Based on Particle Packing Properties, *Chemical Engineering Communications*, **2005**, **192**, 918–932;
- 45. Georgescu, A.M., Platon, N., Arus, V.A., Jinescu, C., Nardou, F., Nistor, I.D.: Study on the Preparation and Characterization of Aluminum-Pillared Clays using Montmorillonite K10, Scientific Study and Research-Chemistry and Chemical Engineering Biotechnology Food Industry, 2023, 24 (2), 145-153;
- Mirila, D.C., Raducanu, D., Georgescu, A.M., Rosu, A.M., Ciubotariu, A.V., Zichil, V., Nistor, I.D.: Silver Nanoparticles Incorporated on Natural Clay as an Inhibitor against the New ISO SS Bacteria Isolated from Sewage Sludge, Involved in Malachite Green Dye Oxidation, *Molecules*, 2022, 27 (18);
- 47. Al-Ghurabi, E.H., Ajbar, A., Asif, M.: Improving Fluidization Hydrodynamics of Group C Particles by Mixing with Group B Particles, *Applied Sciences*, **2018**, **8** (9), 1469, https://doi.org/10.3390/app8091469
- 48. Ursu, A.V., Djelveh, G., Gros, F., Jinescu, G.: Hydrodynamique des Mélanges Ségregatifs en Fluidisation sous Champ Magnétique Transverse et Coaxial, *Récents Progrès en Génie des Procédés*, no. 101, Ed. SFGP, Paris, France, **2011**;
- Hortolomeu, A., Mirila, D.-C., Georgescu, A.-M., Rosu, A.-M., Scutaru, Y., Nedeff, F.-M., Sturza, R., Nistor, I. D.: Retention of Phthalates in Wine using Nanomaterials as Chemically Modified Clays with H<sub>20</sub>, H<sub>30</sub>, H<sub>40</sub> Boltron Dendrimers, *Nanomaterials*, 2023, 13 (16), 2301, https://doi.org/10.3390/nano13162301
- 50. Georgescu, A.M., Nardou, F., Zichil, V., Nistor, I.D.: Adsorption of Lead(II) Ions from Aqueous Solutions onto Cr-Pillared Clays, *Applied Clay Science*, **2018**, **152**, 44-50;
- 51. Muntianu, G., Georgescu, A.M., Nistor, I.D., Jinescu, G.: Ammonia Adsorption Kinetics on Clay Particles in Fluidized Bed, *Bulletin of Romanian Chemical Engineering Society*, **2016**, **3** (2), 2-11;
- 52. Ulusoy, U.: A Review of Particle Shape Effects on Material Properties for Various Engineering Applications: From Macro to Nanoscale, *Minerals*, **2023**, **13** (1), 91, https://doi.org/10.3390/min13010091
- 53. Muntianu, G., Nistor, I.-D., Mirilă, D.-C., Georgescu, A.-M., Aruş, V.-A., Platon, N., Jinescu, C.: Electromagnetic Field Application in Fluidization of Metallic Particles, *Scientific Study & Research Chemistry & Chemical Engineering, Biotechnology, Food Industry*, **2024**, <u>25</u> (4), 439-454:
- 54. Asif, M.: Minimum Fluidization Velocities of Binary- Solid Mixtures: Model Comparison, World Academy of Science, *Engineering and Technology*, **2010**, **4**, 165-169;
- 55. Wen, C.Y., Yu, Y.H.: A Generalized Method for Predicting the Minimum Fluidization Velocity, *A.I.Ch.E. Journal*, **1966**, 610-612;

- 56. Formisani, B. Girimonte, R., Experimental Analysis of the Fluidization Process of Binary Mixtures of Solids, *KONA Powder and Particle Journal*, **2003**, **21**, 66-75.
- 57. Muntianu, G., Georgescu, A.M., Rosu, A.M., Platon, N., Arus, V.A., Jinescu, C.V., Nistor, I.D.: Ammonia Gas Adsorption in Fixed Bed and Fluidized Bed Using Bentonite Particles, *Applied Sciences*, 2025, 15, 832; <a href="https://doi.org/10.3390/app15020832">https://doi.org/10.3390/app15020832</a>.

St. Cerc. St. CICBIA 2025 26 (1)